Remote sensing of urban thermal environments within local climate zones: A case study of two high-density subtropical Chinese cities

Xiaoliang Chen[a,b], Yong Xu[a,b,c,*], Jinxin Yang[c], Zhifeng Wu[c], Hong Zhu[a,b]

[a] Center for Human Geography and Urban Development, School of Geographical Sciences, Guangzhou University, Guangzhou 510006, China
[b] Guangdong Provincial Center for Urban and Migration Studies, Guangzhou 510006, China
[c] Department of Geographical Information Science, School of Geographical Sciences, Guangzhou University, Guangzhou 510006, China

A B S T R A C T

A comprehensive understanding of urban thermal environments is vital for improving urban planning and design strategies to mitigate the urban heat island effect as part of sustainable development. This study investigates the fine-scale thermal environment within high density cities using multi-sourced open satellite data. The whole urban area was first classified based on the urban features such as building morphology and land cover, using the local climate zone scheme; then the thermal performance of different local climate zones was assessed using thermal satellite data. Experiments conducted in two high-density Chinese cities indicated that different urban structures have contrasting thermal conditions in the daytime and nighttime. Furthermore, the utility of different satellite data for detecting and monitoring intra-urban thermal environments was assessed. It was found that Landsat and ASTER satellite data have similar performance, and both datasets perform better than MODIS data, which tend to underestimate urban heat islands. The findings of this study can provide a fast and efficient way to understand the thermal environment within high-density cities, which will allow for better planning to improve urban thermal conditions and ensure more sustainable development.

1. Introduction

Increased urbanization and population growth have degraded the urban ecosystem, particularly the urban thermal environment, which negatively affects public health and energy security (Goggins et al., 2012; Chan et al., 2013). This phenomenon is more significant for rapidly growing Chinese cities, which are denser than many Western cities; the result, together with huge population sizes, causes severe climatic issues, including intensified urban heat islands and worsening ventilation (Ng and Ren, 2015). Thus, a comprehensive understanding of the intra-urban thermal environment is vital for high-density cities to achieve sustainable development.

In the early 1980s, some urban thermal studies have tended to focus on the temperature difference between urban and surrounding rural areas, which results in urban heat islands (UHIs) (Oke, 1981). Oke (1973) pioneered the use of meteorological observation data to understand the causes and mechanisms of UHIs. One of their notable findings was that the intensity of UHIs is highly associated with city size and population. With the advance of remote sensing technology, which offers fast data acquisition and large coverage, satellite data have been widely used to study the principles of UHI and methods for mitigation (Voogt and Oke, 2003; Weng, 2009; Bechtel and Daneke, 2012; Zhan et al., 2013; Mills et al., 2015; Ching et al., 2018). Cutting-edge studies have focused on the spatial-temporal variations of the intra-urban thermal environment and its associations with multi-scale urban landscapes (Connors et al., 2013; Hu et al., 2016; Krayenhoff et al., 2018).

Given that different urban landscapes within a city exhibit different thermal characteristics, conventional UHI studies based on

---

the urban versus rural landscape classification cannot fully describe thermal contrasts within different urban structures (Stewart and Oke, 2012). Thus, in 2012, a new classification system called "local climate zones" (LCZs) was proposed. Based on this system, the whole city area can be classified into 17 standard classes according to land surface conditions, such as building height, cover, fabric, and metabolism. The LCZ system provides a standard way to measure thermal conditions within different urban structures among global cities.

Based on temperature observations and model simulations, the scientific community has confirmed that there are significant temperature contrasts between different LCZs (Stewart et al., 2014; Leconte et al., 2015; Tsin et al., 2016; Geletič et al., 2016; Wang et al., 2018; Bechtel et al., 2019). In particular, Geletič et al. (2016) investigated the land surface temperature (LST) contrasts within LCZs for two European cities using Landsat data. Koc et al. (2018) used high-resolution airborne data to understand the surface temperature characteristics within LCZs for an Australian city, and found that daytime and nighttime thermal characteristics were different for some LCZ classes. In particular, the nighttime thermal characteristics of Sydney, Australia, were found to be similar to the results for the Chinese city of Shanghai (Cai et al., 2018; Koc et al., 2018). Given that temperature contrasts among LCZs for different cities might vary for cities with distinct geographical locations, sizes, and climatic backgrounds, more validation is still necessary (Zhou et al., 2019).

To better understand the thermal environment within different urban structures and provide comprehensive and valuable thermal characteristics within different urban structures, particularly for high-density Chinese cities, in this study we explore diurnal and nocturnal thermal characteristics within local climate zones of high-density cities using multiple satellite data. Furthermore, the performance of different satellite data in detecting intra-urban thermal environments is compared and assessed. The knowledge obtained about the thermal characteristics of different urban structures can benefit planers and policy makers in devising appropriate spatial design strategies to mitigate hotspots in urban areas.

2. Material and method

2.1. Study area

This study focuses on two high-density Chinese cities, Hong Kong and Guangzhou. The locations of these cities are shown in Fig. 1. Hong Kong is located at the mouth of the Pearl River Delta (PRD) in Southern China, while Guangzhou is located in the north of the PRD region. Hong Kong is a Special Administrative Region of the People's Republic of China, with a prosperous economy; it is ranked the seventh largest trading economy in the world. Guangzhou is the capital of Guangdong province in China, and its economy
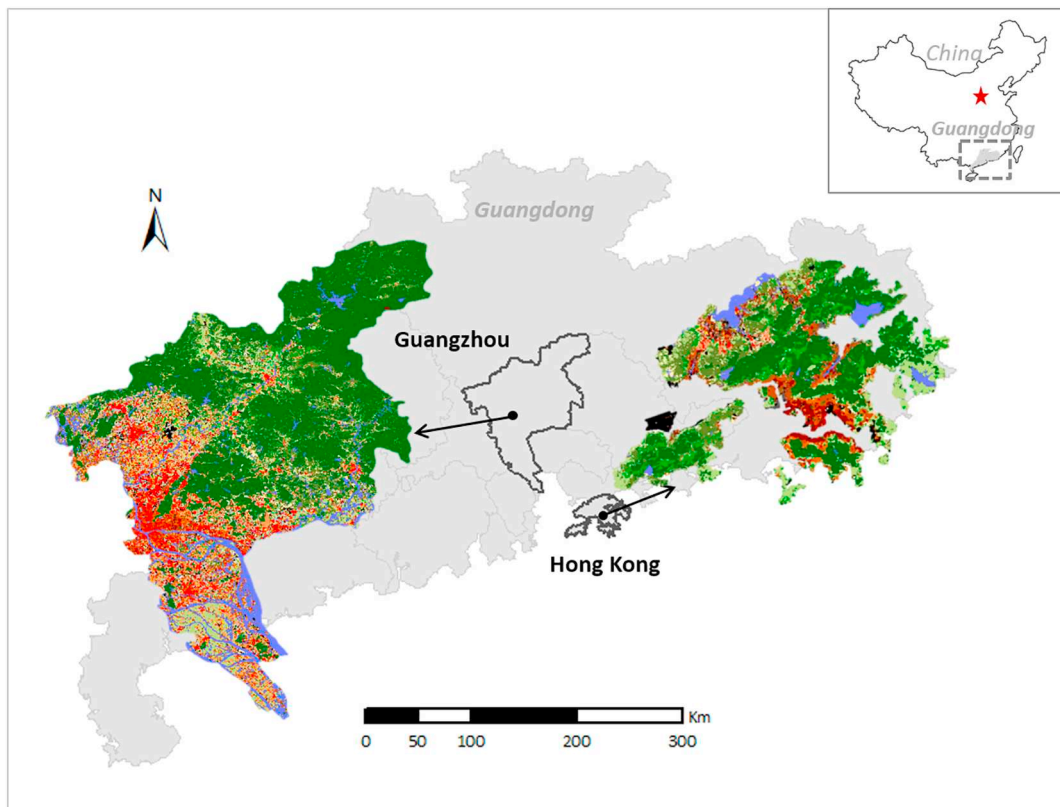
Fig. 1. Locations of Hong Kong and Guangzhou in China.

Table 1
Data description.

Cities	Landsat	MODIS	ASTER
Hong Kong	LT20141015 (day)	MOD20130804 (night) MOD20141015 (day)	AST20130804 (night)
Guangzhou	LT20141015 (day)	MOD20141007 (day) MOD20151020 (night)	AST20141007 (day) AST20151020 (night)

is among the top four in China.

Hong Kong and Guangzhou are typical high-density subtropical Chinese cities, and both cities suffer from extremely hot temperatures in summer and dry winters (Xiong et al., 2012; Yang et al., 2013). The mean annual temperature in Guangzhou is 23 °C, while this figure in Hong Kong is 24 °C. Both have a rainy season from April to September, and half of a years' precipitation generally accounts for > 80% of annual precipitation. The mean annual precipitation in Guangzhou and Hong Kong is 1538 mm and 2234 mm, respectively. Historical statistical data in Hong Kong indicated that the number of very hot days (above 33 °C) has increased from 19 days per year from 2005 to 2014 to 33 days per year between 2014 and 2018. (www.hko.gov.hk/cis/statistic/vhotday_statistic_e. htm). Based on meteorological and public health data, local studies have confirmed a significant relationship between temperature patterns and higher mortality rates, and the harmful effects on suffers from respiratory and cardiovascular aliments (Goggins et al., 2012; Chan et al., 2013). Thus, the choice of these two cities can provide a comprehensive understanding of urban thermal environments in high-density Chinese cities, which can benefit strategies to reduce the negative impact of high temperatures on public health. The findings can also benefit other cities around the world.

2.2. Data input

The data used here include MODIS, Landsat, and ASTER satellite data for both cities (shown in Table 1), and the weather conditions for the overpass dates of the used satellite data are provided in Table 2. Landsat and ASTER data provide medium-resolution thermal information over the study area (at tens of meters per pixel), while MODIS data provide high temporal but coarse resolution thermal bands. All satellite data were processed into standard land surface temperature products. Then, based on all land surface temperature results from multiple satellite data, surface temperature characteristics within different local climate zones were investigated, and the performance of different satellite data were compared and assessed.

Other than the acquired satellite data, vehicle-based air temperature measurement data was also employed to validate the air temperature characteristics within different local climate zones. The mobile measurement data was collected during the summertime at Hong Kong, including both daytime (09:00–11:00) and nighttime (19:00–21:00) data on 17 July 2016, 23 July 2016, 24 Aug 2016, 25 Aug 2016, 27 Oct 2016, and 15 Aug 2017. To reduce the spatial and temporal variations of air temperature measurements, all the measurement routes at different dates were processed and calibrated using nearby weather station data. Details about the mobile measurement data processing and calibration can refer to Shi et al. (2018).

3. Method

3.1. Local climate zones (LCZs)

Local climate zones (LCZs) are a classification system (Stewart and Oke, 2012; Stewart et al., 2014) for urban structures that can promote uniform climate-related classifications of urban and rural field sites for temperature observations (See Fig. 2). The classification system is defined according to regions of consistent land cover, buildings, construction materials, and human activity, covering areas from hundreds of meters to several kilometers. It is local in scale, climatic in nature, and zonal in representation (Stewart and Oke, 2012). Each LCZ class is distinguished by one property related to surface characteristics, such as the height of objects or the majority of land cover.

The standard LCZ classification method proposed by Bechtel et al., 2015 was adopted in this study to generate LCZ maps for both cities. The procedure includes four stages: first, Landsat satellite data were acquired and preprocessed for the study area; second, training areas were selected via the Google Earth platform; third, based on the provided training areas and spectral features from

Table 2
Weather conditions at the overpass dates from Hong Kong Observatory.

	Mean temperature (deg. C)	Mean relative humidity (%)	Total rainfall (mm)	Sunshine hours (hours)	Wind speed[a] (m/s)
20130804	29.2	79	< 0.05	6.5	1.2
20141007	26.3	64	0	10.3	2.1
20141015	25.3	68	0	9.7	1.7
20151015	25.2	76	0	9.1	1.0
20151020	26.2	58	0	7.5	1.3

[a] Records from Shatin station.
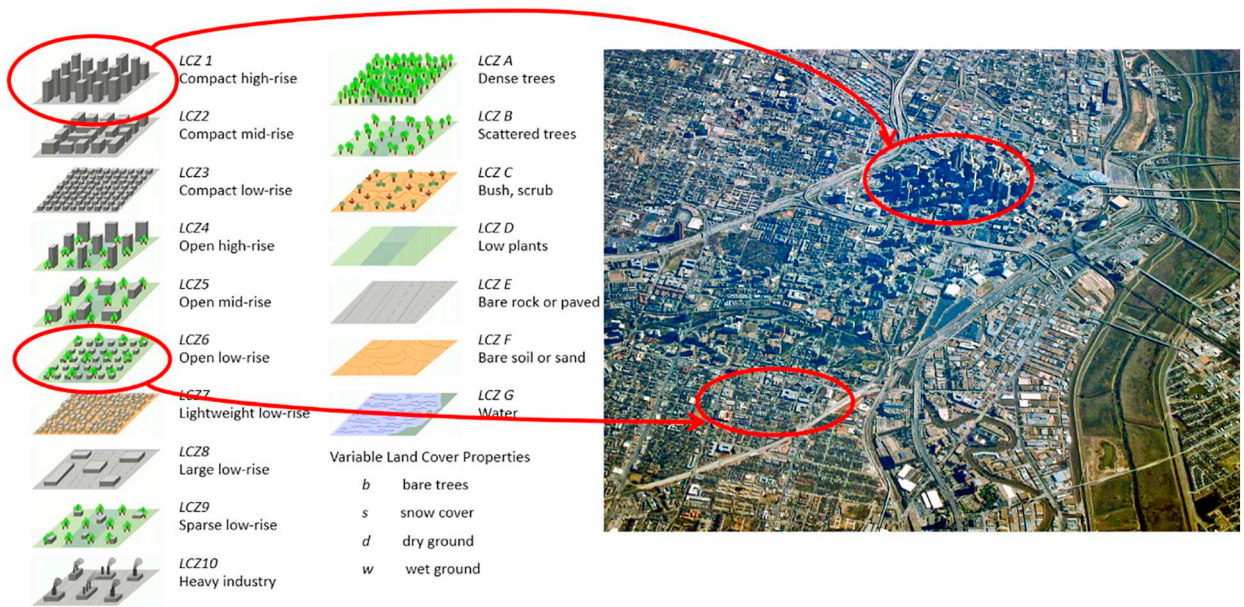
Fig. 2. Scheme of local climate zones (Stewart and Oke, 2012).

satellite data, a random forest classifier was used to classify the whole study area into different LCZ classes; finally, the LCZ mapping result was validated using the obtained validation samples.

3.2. Land surface temperature retrieval

Landsat-8, ASTER, and MODIS data were used to generate land surface temperature results for both study areas, given that all these data are freely accessible. For Landsat data, a single channel algorithm was used to generate land surface temperature results using thermal band 10 from Landsat 8 data, given that thermal band 11 has some calibration issues (Jiménez-Muñoz et al., 2014). For ASTER data, the AST_08 land surface temperature data product was used, from which surface temperature was obtained using a temperature-emissivity separation (TES) algorithm with five thermal infrared (TIR) bands in the 8 and 12 μm spectral range (Gillespie et al., 1998). For MODIS data, the MOD11A2 8-day composite land surface temperature product released by NASA was used, and a split window algorithm was adopted to generate the surface temperature product (Wan et al., 2002). The MOD11A2 LST product has been validated with a high accuracy of about 1 K for general areas (Wan, 2008).

4. Results

4.1. LCZ mapping results

Based on the standard LCZ classification method, the mapping results for Hong Kong and Guangzhou were generated; they are provided in Figs. 3 and 4. High-quality validation data from Google Earth platform for both cities showed that the overall accuracies
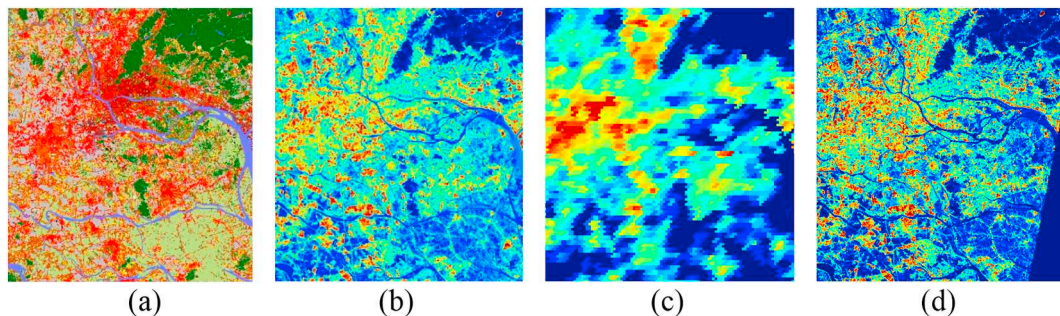
Fig. 3. LCZ map and examples of thermal satellite data for the study area of Guangzhou. (a) LCZ map of Guangzhou; (b) Land surface temperatures obtained from daytime Landsat data on Oct. 15, 2014; (c) Land surface temperatures obtained from 8-day composite MODIS data on Oct. 7, 2014; (d) Land surface temperatures obtained from daytime ASTER data on Oct. 7, 2014.
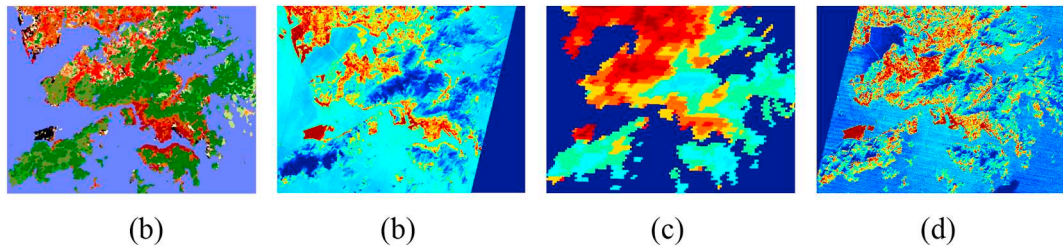
Fig. 4. LCZ map and examples of thermal satellite data for the study area of Hong Kong. (a) LCZ map of Hong Kong; (b) Land surface temperatures obtained from daytime Landsat data on Oct. 15, 2014; (c) Land surface temperatures obtained from 8-day composite MODIS data on Oct. 15, 2014; (d) Land surface temperatures obtained from daytime ASTER data on Nov. 31, 2016.

for Guangzhou and Hong Kong were about 70% and 60%, respectively (Xu et al., 2017; Wang et al., 2018). Visual evaluation also indicates that the LCZ results can well reflect actual land cover distributions for both cities. Taking the LCZ mapping result for Guangzhou (provided in Fig. 3) as an example, the main urban area in the north of the image is well classified as a high-density urban area (highlighted in red), except for the center urban area. Some red and orange color clusters can be seen in the south and southwest of Guangzhou, which represent satellite cities such as Foshan and Shunde. Other than LCZs 1–3, some open building settlements marked in orange (LCZs 4–6) are located in the suburbs of each city. Most of the remaining areas are classified as low plants (LCZ D) or dense trees (LCZ A), which are highlighted in light blue and dark green, respectively.

Compared with Guangzhou, Hong Kong is small and has no satellite cities. The center of Hong Kong includes Kowloon Peninsula and Hong Kong Island, separated by Victoria Harbor. The majority of the center of Hong Kong is classified as high-density, high-rise buildings (LCZ 1) in dark red, and only part of the center area was classified as other types of high-density buildings (e.g., LCZs 2–3). In the suburbs of Hong Kong, there are some suburban towns indicated by light red, particularly in the north. Other than a few towns, most of the suburbs are covered by dense trees (LCZ A) and low plants (LCZ D). Because most of Hong Kong's natural land belongs to country parks, the areas with natural LCZ types such as dense trees and low plants should be similar to country park areas. Compared with Guangzhou, the proportion of natural LCZ types (~70%) is higher in Hong Kong than in Guangzhou (~50%).

4.2. Land surface temperature results

Based on the acquired multiple satellite data, three sets of land surface temperature result for both Guangzhou and Hong Kong were obtained, in which the LST results using ASTER or Landsat data have a resolution of 100 m, while the LST data with MODIS data have a resolution of 1 km. To ensure both LST and LCZ data are comparable, the LST data were resampled at 100 m.

Based on the land surface temperature results shown in Figs. 3 and 4, it is apparent that the thermal patterns found in different satellite data are quite similar. In terms of the daytime LST in Guangzhou, for example, high surface temperatures occur in the north and eastern areas according to both Landsat and MODIS satellite data. We also note that high surface temperatures can occur in natural LCZ types during the daytime, as some areas in the northwest suburbs of Hong Kong show high surface temperatures.

4.3. Land surface temperature and local climate zones

Based on the derived LST and LCZ results, typical mean LSTs for each LCZ types can be obtained. Indices including the mean LST and the variance of each LCZ type can be calculated. The distributions of LST per LCZ using different satellite data for Guangzhou and Hong Kong are provided in boxplots in Figs. 5 and 6.

Based on these results, it is apparent that the associations between LSTs and LCZs for both cities are consistent. The high-density urban LCZ classes (LCZ1–3) tend to have higher land surface temperatures, while the natural LCZ classes tend to have lower surface temperatures (e.g., LCZ A-D). In addition, we found that the associations between LCZs and LSTs were quite different between day and night. In particular, high surface temperatures in the daytime were obtained for high-density low-rise buildings (e.g., LCZ 3), while in the nighttime, high surface temperatures were obtained for high-density high-rise buildings (e.g., LCZ 1).

We performed a one-way ANOVA F-test ($p < .01$) to determine whether there were significant differences between the average LSTs of various LCZs. Fig. 7 shows the comparative results for the mean LSTs of LCZs in Guangzhou and Hong Kong using Landsat and ASTER data, in which gray values represent a "negative" result, meaning that there is no difference between LSTs for a given pair of LCZs, while empty spaces with "*" or "**" represent a "positive" result, indicating a significant differences between pairs of LCZs. It is apparent that statistically significant temperature differences between LCZs prevail in both study areas, for both diurnal and nocturnal observations. It can also be observed that the temperature difference within LCZs was more significant in the daytime, as > 96% and 93% of LCZ pairs in the cities passed the test during the day, but the values during the night were 94% and 89%, respectively. Compared with Guangzhou, the difference test results in Hong Kong showed less variation (e.g., 89% vs 93% for the nighttime). The main reason might be the marine climate of Hong Kong, as it is much closer to the ocean. Thus, the background climate is more easily affected by the ocean, which means that the temperature difference of Hong Kong is less significant than in Guangzhou.
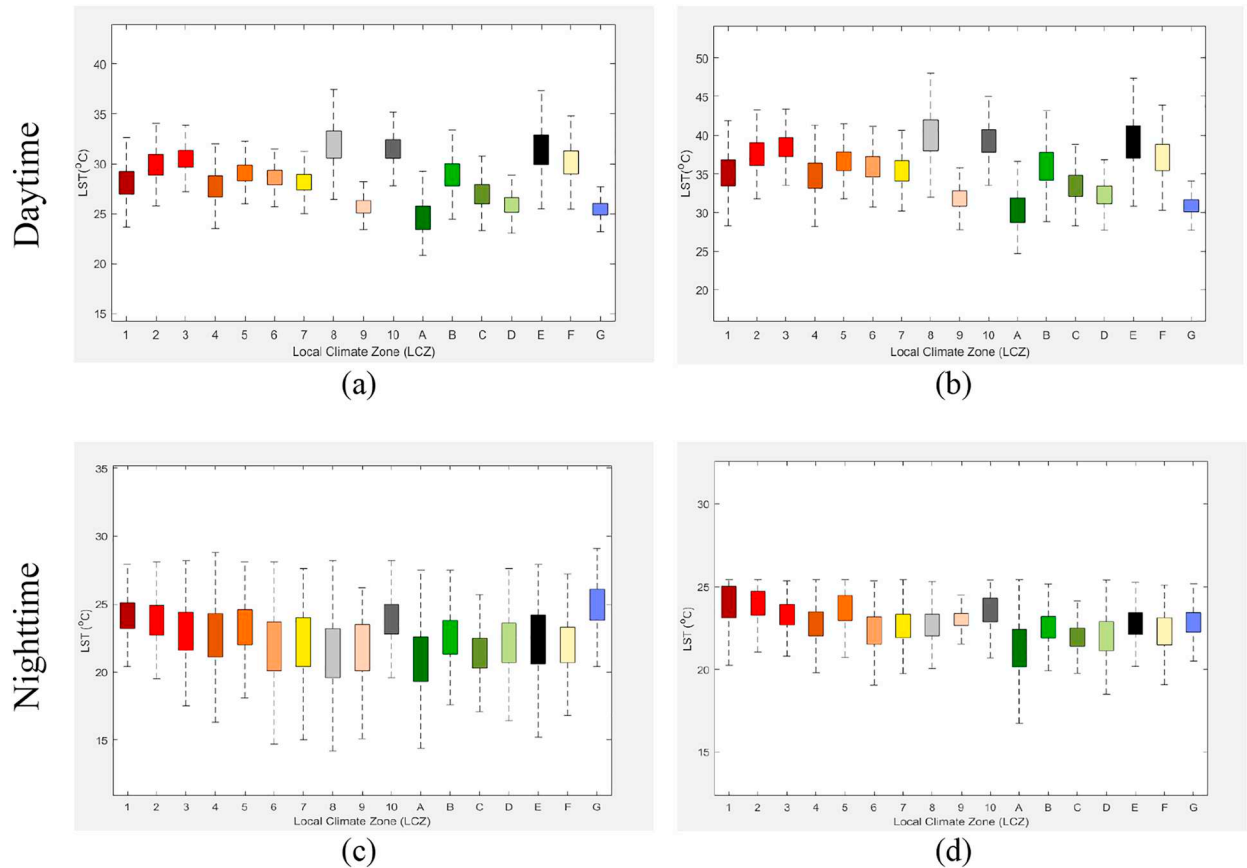
Fig. 5. Boxplots of LSTs in LCZ classes in Guangzhou for daytime and nighttime, using (a) Landsat data (daytime, Oct. 15, 2014); (b) ASTER data (daytime, Oct 7, 2014); (c) ASTER data (nighttime, Oct. 20, 2015); (d) MODIS data (nighttime, Oct. 20, 2015).

5. Results and discussion

5.1. Daytime thermal environment of different local climate zones

Based on daytime images and vehicle-based measurement data, the association between thermal environments and different LCZ types presented in Fig. 8 (a). It can be easily seen that the daytime thermal pattern of different LCZ classes for both Guangzhou and Hong Kong is similar. Generally, urban LCZ types (e.g., LCZs 1–8) tend to have higher land surface temperatures than natural LCZ types (e.g., LCZs A-D). The reasons include vegetation and moist soil among natural LCZ types, which can slow down the heating-up process during the daytime. Other than urban LCZ types, there are still a few natural LCZ types, like LCZ E (bare land), that have higher surface temperatures during the daytime. The reason might be the thermal properties of bare land in the suburbs, which can heat up very quickly during the day.

Comparison of the thermal environment within the urban LCZ categories shows that the dense urban morphology (e.g., LCZs 2–3) generally has higher surface temperatures than open urban morphology (e.g., LCZs 4–6). The reason might be that open urban morphology has some vegetation and soil, which can slow down the warming-up process. Comparison of the high-density LCZ categories shows that high-density low-rise buildings tend to have higher daytime surface temperatures than the other high-density categories, including high-density high- and mid-rise buildings (LCZs 1 and 2). The reason might be the large thermal load as well as the shading effect of high-density high- and mid-rise building morphology, which can restrain the heating-up process better than the high-density low-rise buildings. Compared with the open LCZ categories, LCZ 5 (open mid-rise) tends to have higher surface temperatures than the other open categories (e.g., LCZ 4 high-rise or LCZ 6 low-rise). However, the difference within open LCZ categories is minor compared with the difference between dense and open LCZ categories.

Moreover, high-rise LCZ classes perform slightly different in the cities, as open high-rise buildings in Guangzhou tends to have lower surface temperatures than other urban LCZ categories. However, open high-rise buildings in Hong Kong are comparable to other types of open buildings. One possible reason is that the coverage ratio of vegetation and open space within open high-rise buildings in Guangzhou is higher than those in Hong Kong, thus leading to a larger cooling and shading effect, so that the surface temperature is cooler than for other LCZ types.
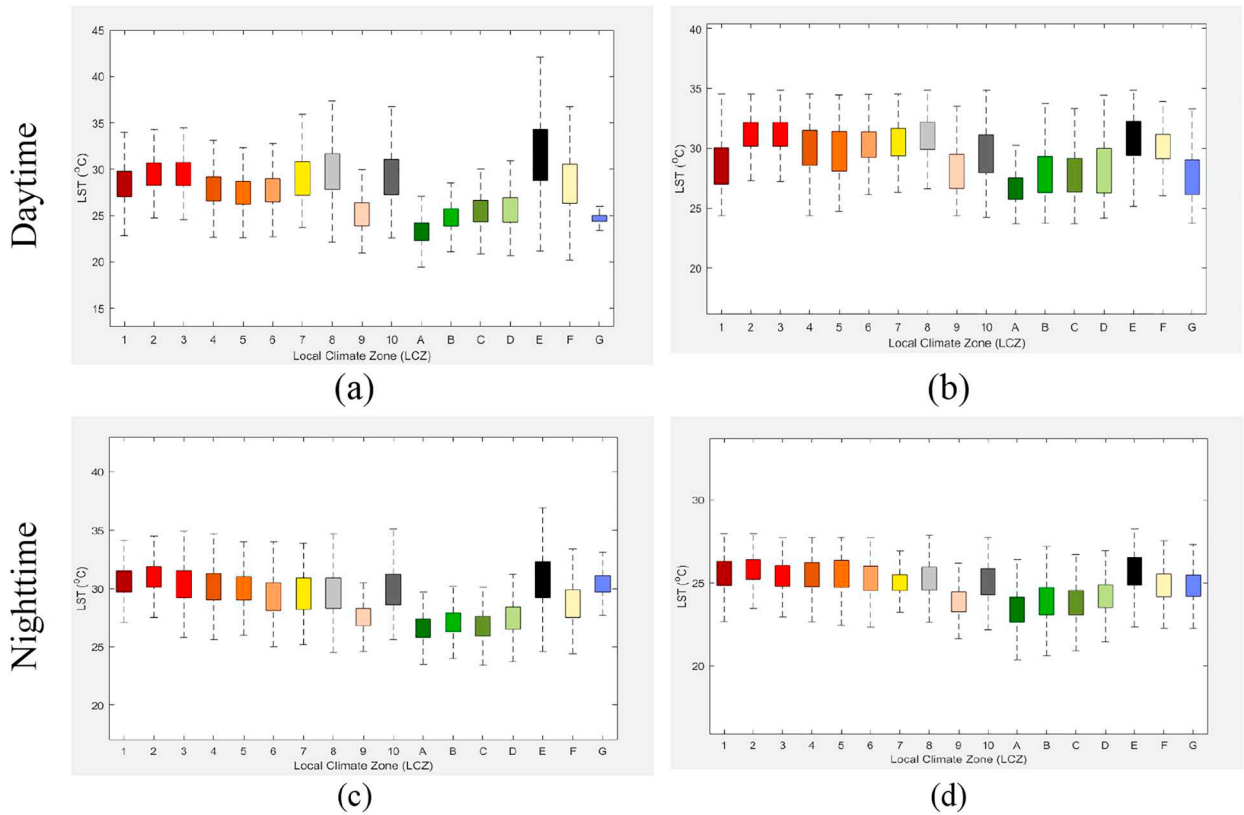
Fig. 6. Boxplots of LSTs in LCZ classes in Hong Kong for daytime and nighttime, using (a) Landsat data (daytime, Oct. 15, 2014); (b) MODIS data (daytime, Oct. 15, 2014); (c) ASTER data (nighttime, Aug. 4, 2013); (d) MODIS data (nighttime, Aug. 4, 2013).
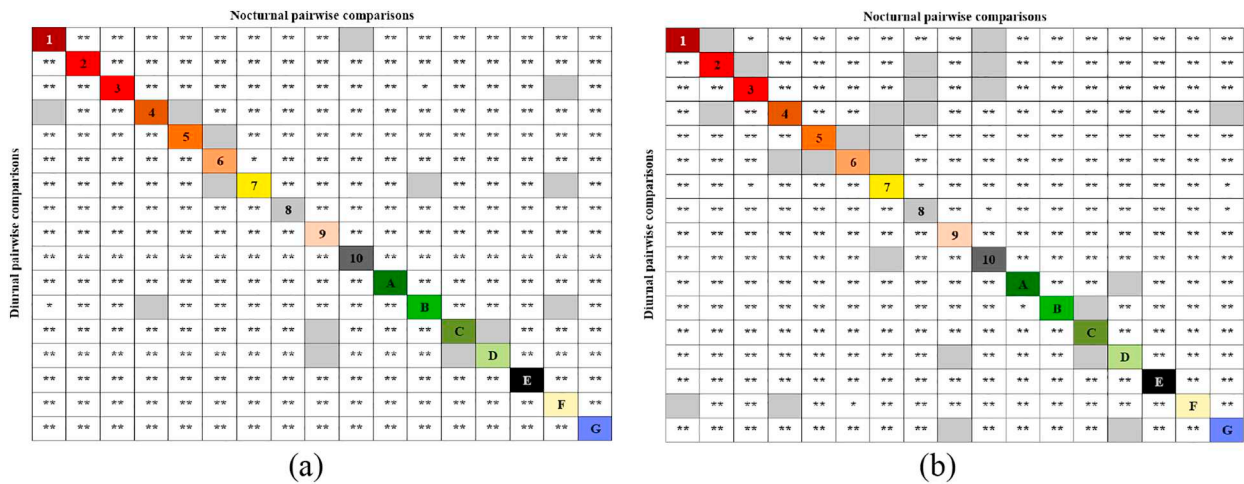
Fig. 7. Binary matrix showing the diurnal and nocturnal temperature difference tests for Guangzhou and Hong Kong (empty cells indicate that the LSTs within pairs of LCZs were significantly different, while gray cells indicate that the LSTs within pairs of LCZs were not significantly different): (a) Test results for Guangzhou; (b) Test results for Hong Kong.

5.2. Nighttime thermal environment of different local climate zones

The association between nighttime LST and LCZ types for Guangzhou and Hong Kong is presented in Fig. 8 (b). Compared with thermal patterns in the daytime, the main difference is that some urban LCZ categories (e.g., LCZ 1) with a high thermal load tend to have a greater surface temperature at night than in the day. For example, LCZ 1 with high-density high-rise buildings tends to have lower surface temperatures in the daytime, but it almost reaches the highest levels during the nighttime. Moreover, some LCZ categories with relatively high surface temperatures tend to cool down at night, such as LCZ 3 and LCZ 8. The reason might be the
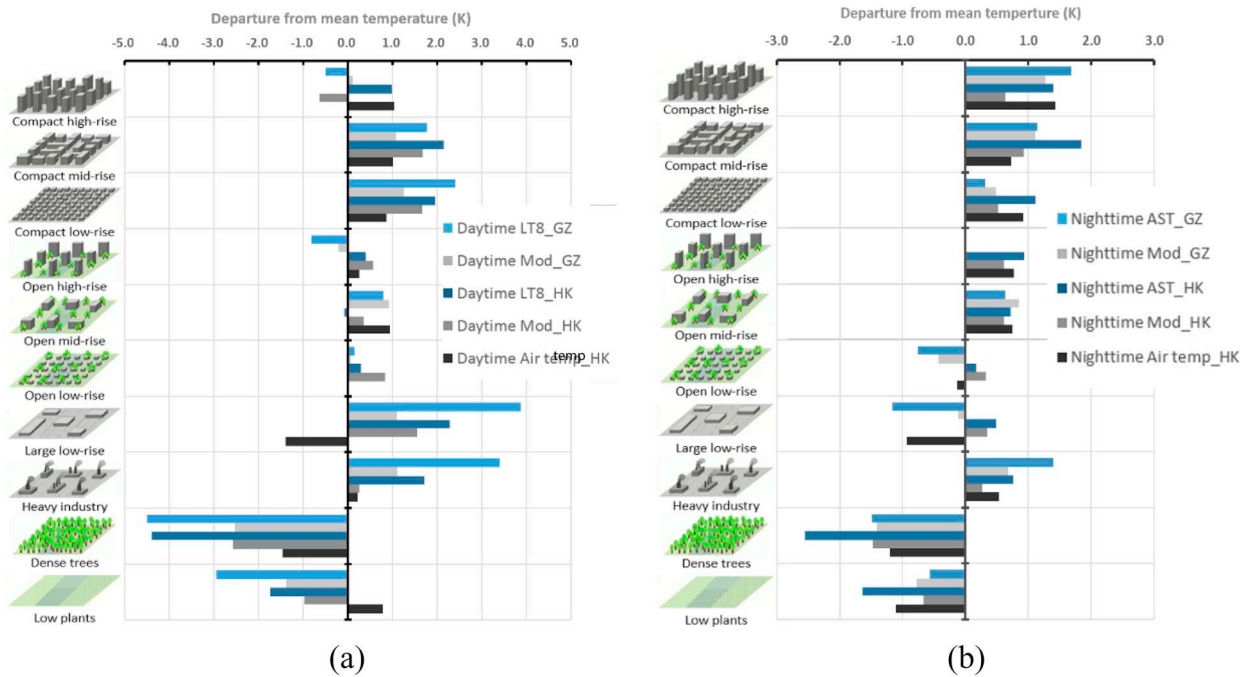
Fig. 8. Daytime and nighttime thermal differentiation of local climate zones for Guangzhou (GZ) and Hong Kong (HK) using multiple thermal satellite data: (a) Daytime thermal differentiation; (b) Nighttime thermal differentiation.

lower thermal load of low-rise buildings and good ventilation conditions, so that they tend to cool down much faster than other LCZ classes.

In both cities, the high-density high-rise LCZs tend to have higher nighttime surface temperatures than the open low-rise LCZs. In particular, the high-density high- and mid-rise LCZs have higher surface temperatures than other urban LCZ categories. Nevertheless, in Guangzhou, LCZ 1 with high-density high-rise buildings has the highest nighttime surface temperature, while in Hong Kong, high-density mid-rise buildings tend to have the highest nighttime surface temperature according to the satellite data. The reason might be that there was a strong land-sea interaction (e.g., sea breeze) of Hong Kong at the observation time, so that the high-density high-rise buildings can cool down much faster than the other building types.

5.3. Evaluation of different sensors

The performance of different sensors (including Landsat, ASTER, and MODIS) in detecting the thermal environment of LCZs was
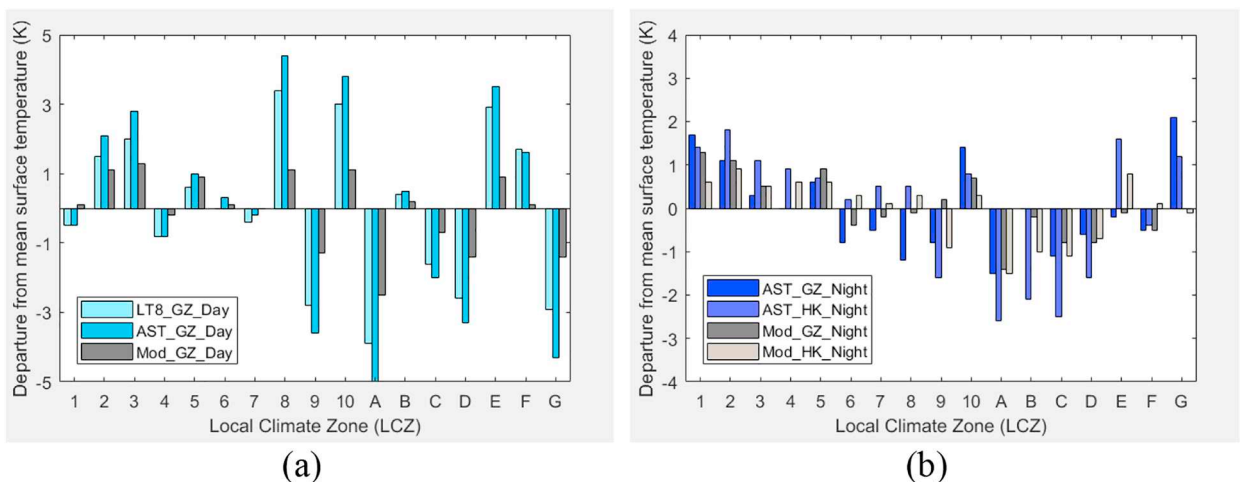
Fig. 9. Thermal performance with different satellite data in daytime and nighttime: (a) daytime LSTs in LCZ classes for Guangzhou using different satellite data; (b) nighttime LSTs in LCZ classes for Guangzhou and Hong Kong using different satellite data.

also assessed. To ensure a fair comparison, images acquired on nearly the same date were tested. Fig. 9(a) shows the associations between LSTs and LCZs in the daytime for Guangzhou using Landsat, ASTER and MODIS data, while Fig. 9(b) shows the associations between LSTs and LCZs at night for Guangzhou and Hong Kong using ASTER and MODIS data. Based on the results, it is apparent that LST patterns within LCZs using Landsat or ASTER data were quite similar, as LCZs 2, 3, 8, and 10 have higher surface temperature during the day, while some natural LCZ types (e.g., LCZ A) tend to have relatively lower surface temperatures due to their different thermal properties.

The performance of different satellite data was assessed by estimating the surface UHIs (SUHI) for both cities. Let us assume that daytime SUHI can be estimated by the LST difference between LCZ 3 and LCZ A. Then, based on the daytime LSTs shown in Figs. 9(a), it can be inferred that the daytime SUHIs for Guangzhou were 5.9 and 7.9C when Landsat or ASTER were used, while the daytime SUHI was 3.8 when MODIS LST data was used. Similarly, if the nighttime SUHI can be simplified as the average LST difference between LCZs 1–2 and LCZ A, the nighttime SUHIs of Guangzhou and Hong Kong can be estimated as 3.2 and 4.4C using ASTER data, while the nighttime SUHIs were 2.7 and 2.4C using MODIS data. Thus, it is apparent that both nighttime and daytime SUHIs were underestimated by MODIS compared with Landsat or ASTER. The underestimation for both cities was about 1–4C, and the daytime SUHI was more seriously underestimated than the nighttime.

The performance of different satellite data was also assessed by detecting the temperature difference between LCZs. As indicated in Fig. 9, the order of surface temperature for different LCZs using ASTER or Landsat data is quite similar, as LCZ 2, 3, 8, and 10 have relatively high surface temperature, and LCZ 5, 6, 1, and 4 have medium-level surface temperatures; natural LCZ types have the lowest surface temperatures (e.g., LCZ A). The statistical test results also indicate that the thermal difference for most pairs of LCZs is significant using Landsat or ASTER data, and their performance is similar. However, the temperature difference between pairs of LCZs is less significant when MODIS data are used. As indicated in Fig. 9, the LSTs between LCZ 2 and LCZ 5 are significantly different using either Landsat or ASTER data, but the difference is less significant when MODIS data are used. Thus, Landsat and ASTER have better performance than MODIS in detecting thermal differences between pairs of LCZs.

5.4. Limitations

One limitation of our study is that the effect of urban canyon as well as the urban wind environment can alter the thermal performance of different LCZs, which has not been considered in this study. To better understand the LST-LCZ associations, model-based approaches might be required to explore the impact of urban ventilation on the thermal characteristics within different LCZs. Other than urban canyon, different archetypes as well as urban materials are also ignored in this study. Experimental results indicated that some LCZ classes have large intra-class temperature variance, one possible reason might be due to the diverse archetypes and urban materials within the same LCZ class. Moreover, the air temperature difference between LCZ classes was found not as significant as the surface temperature difference using satellite data, a preliminary explanation might be due to the combined effects of the coastal nature and high-rise and compact urban morphology, which needs further investigation.

6. Conclusion

This study investigated the combination of multi-sourced satellite data to analyze the thermal characteristics of LCZs in high-density cities. Experimental results indicated significant LST differences between pairs of LCZs. Compared with other LCZs, high-density urban LCZs (e.g., LCZ 1–3) tended to have higher surface temperatures, while natural LCZs with a large percentage of vegetation tended to have lower LSTs. The results also indicated that the LST difference between LCZs in high-density cities was significant, as the number of positive tests for both cities was above 89%.

Other than the contrasting thermal performance within local climate zones, some new findings about associations between LSTs and LCZs in high-density cities can be summarized as follows. First, high-rise urban LCZ classes (e.g., high-density high-rise LCZ 1 and open high-rise LCZ 4) tended to have high surface temperatures at night; nevertheless, their surface temperature was very low during the daytime compared with some other urban LCZ classes. Second, the thermal distribution within a city was quite different between day and night. The results indicated that highest daytime surface temperatures were usually obtained for high-density low-rise urban LCZ classes (e.g., LCZs 3 and 8), while the highest nighttime surface temperature were usually obtained for high-density high- and mid-rise urban LCZ classes (e.g., LCZs 1 and 2). Thus, the high surface temperatures might take place in different parts of the city during the day and night. This finding indicates that nighttime thermal imaging might better characterize the real thermal environment within a city.

In addition, the performance of different satellite data in detecting intra-urban thermal environment was assessed. Medium-resolution satellite data from Landsat and ASTER performed much better than coarse-resolution MODIS data, both in detecting the intensity of unban heat islands and in discriminating the thermal characteristics of different LCZs. In particular, it is found that MODIS data tended to underestimate the urban heat islands in both the day and night, by about several Celsius degree for both cities.

This study analyzed the thermal characteristics of different urban structures in high-density cities. The findings will facilitate the development of spatial strategies to improve urban thermal conditions, particularly in high-density cities. Further studies might make use of street-level thermal comfort questionnaires and public health information to investigate the impact of the urban thermal environment on public health, which is vital for sustainable, healthy urban development.

Declaration of Competing Interest

To the best of our knowledge, all the named authors have no conflict of interest, financial or otherwise.

Acknowledgement

References

Bechtel, B., Daneke, C., 2012. Classification of local climate zones based on multiple earth observation data. IEEE J. Sel. Top. Appl. Earth Obs. Remote Sens. 5 (4), 1191–1202.

Bechtel, B., Alexander, P., Böhner, J., Ching, J., Conrad, O., Feddema, J., ... Stewart, I., 2015. Mapping local climate zones for a worldwide database of the form and function of cities. ISPRS International Journal of Geo-Information 4 (1), 199–219.

Bechtel, B., Demuzere, M., Mills, G., Zhan, W., Sismanidis, P., Small, C., Voogt, J., 2019. SUHI analysis using local climate zones—a comparison of 50 cities. Urban Clim. 28, 100451.

Cai, M., Ren, C., Xu, Y., Lau, K.K.L., Wang, R., 2018. Investigating the relationship between local climate zone and land surface temperature using an improved WUDAPT methodology–a case study of Yangtze River Delta, China. Urban Clim. 24, 485–502.

Chan, E.Y., Goggins, W.B., Yue, J.S., Lee, P., 2013. Hospital admissions as a function of temperature, other weather phenomena and pollution levels in an urban setting in China. Bull. World Health Organ. 91, 576–584.

Ching, J., Mills, G., Bechtel, B., See, L., Feddema, J., Wang, X., ... Mouzourides, P., 2018. WUDAPT: An urban weather, climate, and environmental modeling infrastructure for the anthropocene. Bulletin of the American Meteorological Society 99 (9), 1907–1924.

Connors, J.P., Galletti, C.S., Chow, W.T., 2013. Landscape configuration and urban heat island effects: assessing the relationship between landscape characteristics and land surface temperature in Phoenix, Arizona. Landsc. Ecol. 28 (2), 271–283.

Geletič, J., Lehnert, M., Dobrovolný, P., 2016. Land surface temperature differences within local climate zones, based on two central European cities. Remote Sens. 8 (10), 788.

Gillespie, A., Rokugawa, S., Matsunaga, T., Cothern, J.S., Hook, S., Kahle, A.B., 1998. A temperature and emissivity separation algorithm for Advanced Spaceborne Thermal Emission and Reflection Radiometer (ASTER) images. IEEE Trans. Geosci. Remote Sens. 36 (4), 1113–1126.

Goggins, W.B., Chan, E.Y., Ng, E., Ren, C., Chen, L., 2012. Effect modification of the association between short-term meteorological factors and mortality by urban heat islands in Hong Kong. PLoS One 7 (6), e38551.

Hu, L., Monaghan, A., Voogt, J.A., Barlage, M., 2016. A first satellite-based observational assessment of urban thermal anisotropy. Remote Sens. Environ. 181, 111–121.

Jiménez-Muñoz, J.C., Sobrino, J.A., Skoković, D., Mattar, C., Cristóbal, J., 2014. Land surface temperature retrieval methods from Landsat-8 thermal infrared sensor data. IEEE Geosci. Remote Sens. Lett. 11 (10), 1840–1843.

Koc, C.B., Osmond, P., Peters, A., Irger, M., 2018. Understanding land surface temperature differences of local climate zones based on airborne remote sensing data. IEEE J. Sel. Top. Appl. Earth Obs. Remote Sens. 11 (8), 2724–2730.

Krayenhoff, E.S., Moustaoui, M., Broadbent, A.M., Gupta, V., Georgescu, M., 2018. Diurnal interaction between urban expansion, climate change and adaptation in US cities. Nat. Clim. Chang. 8 (12), 1097.

Leconte, F., Bouyer, J., Claverie, R., Pétrissans, M., 2015. Using local climate zone scheme for UHI assessment: evaluation of the method using mobile measurements. Build. Environ. 83, 39–49.

Mills, G., Ching, J., See, L., Bechtel, B., Foley, M., 2015, July. An Introduction to the WUDAPT project. In: Proceedings of the 9th International Conference on Urban Climate, Toulouse, France, pp. 20–24.

Ng, E., Ren, C. (Eds.), 2015. The Urban Climatic Map: A Methodology for Sustainable Urban Planning. Routledge.

Oke, T.R., 1973. City size and the urban heat island. Atmos. Environ. 7, 769–779.

Oke, T.R., 1981. Canyon geometry and the nocturnal urban heat island: comparison of scale model and field observations. Int. J. Climatol. 1 (3), 237–254.

Shi, Y., Lau, K.K.L., Ren, C., Ng, E., 2018. Evaluating the local climate zone classification in high-density heterogeneous urban environment using mobile measurement. Urban Clim. 25, 167–186.

Stewart, I.D., Oke, T.R., 2012. Local climate zones for urban temperature studies. Bull. Am. Meteorol. Soc. 93 (12), 1879–1900.

Stewart, I.D., Oke, T.R., Krayenhoff, E.S., 2014. Evaluation of the 'local climate zone'scheme using temperature observations and model simulations. Int. J. Climatol. 34 (4), 1062–1080.

Tsin, P.K., Knudby, A., Krayenhoff, E.S., Ho, H.C., Brauer, M., Henderson, S.B., 2016. Microscale mobile monitoring of urban air temperature. Urban Clim. 18, 58–72.

Voogt, J.A., Oke, T.R., 2003. Thermal remote sensing of urban climates. Remote Sens. Environ. 86 (3), 370–384.

Wan, Z., 2008. New refinements and validation of the MODIS land-surface temperature/emissivity products. Remote Sens. Environ. 112 (1), 59–74.

Wan, Z., Zhang, Y., Zhang, Q., Li, Z.L., 2002. Validation of the land-surface temperature products retrieved from Terra Moderate Resolution Imaging Spectroradiometer data. Remote Sens. Environ. 83 (1–2), 163–180.

Wang, R., Ren, C., Xu, Y., Lau, K.K.L., Shi, Y., 2018. Mapping the local climate zones of urban areas by GIS-based and WUDAPT methods: a case study of Hong Kong. Urban Clim. 24, 567–576.

Weng, Q., 2009. Thermal infrared remote sensing for urban climate and environmental studies: methods, applications, and trends. ISPRS J. Photogramm. Remote Sens. 64 (4), 335–344.

Xiong, Y., Huang, S., Chen, F., Ye, H., Wang, C., Zhu, C., 2012. The impacts of rapid urbanization on the thermal environment: a remote sensing study of Guangzhou, South China. Remote Sens. 4 (7), 2033–2056.

Xu, Y., Ren, C., Cai, M., Edward, N.Y.Y., Wu, T., 2017. Classification of local climate zones using ASTER and Landsat data for high-density cities. IEEE J. Sel. Top. Appl. Earth Obs. Remote Sens. 10 (7), 3397–3405.

Yang, J., Liu, H.Z., Ou, C.Q., Lin, G.Z., Zhou, Q., Shen, G.C., Chen, P.Y., Guo, Y., 2013. Global climate change: impact of diurnal temperature range on mortality in Guangzhou, China. Environ. Pollut. 175, 131–136.

Zhan, W., Chen, Y., Zhou, J., Wang, J., Liu, W., Voogt, J., Zhu, X., Quan, J., Li, J., 2013. Disaggregation of remotely sensed land surface temperature: literature survey, taxonomy, issues, and caveats. Remote Sens. Environ. 131, 119–139.

Zhou, D., Xiao, J., Bonafoni, S., Berger, C., Deilami, K., Zhou, Y., Frolking, S., Yao, R., Qiao, Z., Sobrino, J., 2019. Satellite remote sensing of surface urban heat islands: Progress, challenges, and perspectives. Remote Sens. 11 (1), 48.